Seismic monitoring of CO2 plume growth, evolution and migration in a heterogeneous reservoir: Role, impact and importance of patchy saturation

Seismic monitoring of CO_2 plume growth, evolution and migration in a heterogeneous reservoir: Role, impact and importance of patchy saturation.

Rami Eid [a]*, Anton Ziolkowski [a], Mark Naylor [a], Gillian Pickup [b]

[a] University of Edinburgh, Edinburgh, EH9 3FE, United Kingdom
[b] Heriot-Watt University, Edinburgh, EH14 4AS, United Kingdom

**Corresponding author. Tel.: +44(0)-758-276-0792; Fax: +44(0)-131-668-3184*
Email address: Rami.Eid@ed.ac.uk

Abstract

We combine reservoir simulation with 2D synthetic seismic reflection time-lapse data to assess the ability of seismic methods to image plume growth, evolution, and migration within a heterogeneous saline reservoir. The incorporation of reservoir heterogeneity results in a range of saturations due to the tortuous migration around the intra-reservoir baffles. To account for the disruptive nature of the injected CO_2, and the uncertainties regarding the fluid saturation distribution, we use two end-member models, uniform and patchy, to generate the widest range of seismic velocity distributions to understand the range of velocity-saturation behaviour which could be encountered. The generated seismic sections show clear differences between the two models while also providing confidence in the ability to detect CO_2 plume growth and evolution in the reservoir. A free-phase migrating front of CO_2 appears to be difficult to detect, however. The ability to image a front is shown to be dependent not only on the pore-fluid saturation distribution - patchy or uniform - but also on its larger-scale spatial geometry. As the subtle change in amplitude is directly related to the concentration of CO_2 within each accumulation, it suggests that the saturation model has important implications for CO_2 detectability and for quantifying the volume of CO_2 injected into the reservoir.

Keywords: CCS, monitoring, migration, time-lapse seismic, rock physics, patchy saturation

1. Introduction

To demonstrate successful containment of injected CO_2 as part of a carbon capture and storage (CCS) project, the operator is expected to monitor, measure and validate the injected CO_2 in the intended formation and, importantly, identify and quantify any movement within the reservoir.

Seismic techniques are commonly used to monitor CO_2 containment over the lifetime of a project (Lumley, 2010). Through the application of time-lapse seismic surveys, pilot CO_2 sequestration sites such as Sleipner (Arts et al., 2004, Arts et al., 2008), Weyburn (Wilson and Monea, 2004) and Ketzin (Bergmann et al., 2011, Ivandic et al., 2012, Ivandic et al., 2015) have successfully monitored structurally trapped CO_2, because the displacement of brine by less dense and more compressible CO_2 results in changes in the acoustic properties of the reservoir (Pearce, 2005). However, the ability to accurately image a free-phase migrating CO_2 plume during injection remains challenging due to uncertainties regarding the pore-scale distribution of fluids within the reservoir, and in turn, the most appropriate rock-physics model to simulate this. As the seismic response depends not only on the fluid type - liquid or gas - but also on the fine-scale spatial distribution of the phases (White, 1975, Mavko and Mukerji, 1998), end-member fluid distribution models are used here to predict the possible range of expected velocities prior to generating and interpreting the seismic response. A free-phase migrating CO_2 plume is defined as CO_2 which is not immobilized by residual or structural trapping.

Fluid-flow to seismic modeling workflows are typically used before, during and after CO_2 injection to determine what a given sensor would measure in a given environment. This is the process through which a subsurface geological model is injected with CO_2 and then transformed into a synthetic seismic record. This tool is used during initial storage-site assessment stages to determine whether the injected CO_2 will generate an interpretable change in signature on processed reflection seismic data. Synthetic records generated during and after injection facilitate the interpretation of the processed data and assist in the process of history matching. Such workflows have been successfully used to history match the migration of the CO_2 plume at Sleipner (Chadwick et al., 2006, Singh et al., 2010, Boait et al., 2012).

Gassmann's equation (Gassmann, 1951) is used almost exclusively for fluid substitution to estimate the effect of fluid changes on elastic properties. However, one of the main assumptions is that the distributed phases are immiscible and homogeneously distributed throughout the pore space (uniform fluid saturation). This assumption is valid for virgin reservoir systems or trapped hydrocarbon accumulations which have come to equilibrium over geological timescales. However, the injection and migration of CO_2 perturbs this equilibrium resulting in a non-uniform distribution. Patchy and Uniform saturation distributions represent two extreme bounds of sub-seismic scale saturation heterogeneity, representing the bulk modulus of the fluid mixture which can then be input directly into Gassmann's equation for modelling (Mavko and Mukerji, 1998). Patchy saturation represents the upper bound of seismic velocities while Uniform saturation represents the lower bounds of seismic velocities as a function of CO_2 saturation (Sengupta and Mavko, 2003, Cairns et al., 2012). These end-member models are used here to generate the widest range of velocities which could be encountered, as the exact relation between the two bounds in the subsurface is usually unknown. Understanding the range of pore-fluid saturation scales and the phase distributions which could be encountered, therefore, is critical when assessing the potential for the detectability of CO_2 migration using seismic techniques.

In this study, we compute the time-lapse seismic responses of a heterogeneous saline reservoir in the UK sector of the North Sea. The incorporation of reservoir heterogeneity results in a range of saturations. This complexity allows for a more representative velocity distribution. To account for the uncertainties regarding the fluid saturation distribution, end-member models – uniform and patchy – are used to generate the widest range of velocity distributions to try to understand the velocity-saturation behaviour which could be encountered. As the range of saturations within a pore space is constrained by limits for irreducible saturation, we have modified the patchy curve, so that it starts from a given irreducible water saturation. The uniform and modified-patchy models are then used to simulate time-lapse seismic responses in order to assess the potential for seismic methods to image CO_2 plume growth and evolution within a reservoir, as well as the potential to detect a free-phase migrating front of CO_2.

2. Methodology

To simulate a migrating plume, and investigate the range of seismic responses due to the injected CO_2, we model variations in the time-lapse signal over a heterogeneous sandstone reservoir through the application of a three-stage model-driven workflow. This consists of fluid-flow modelling, rock physics modelling and seismic forward modelling, as illustrated in Fig. 1. We now describe the different stages in the modelling.

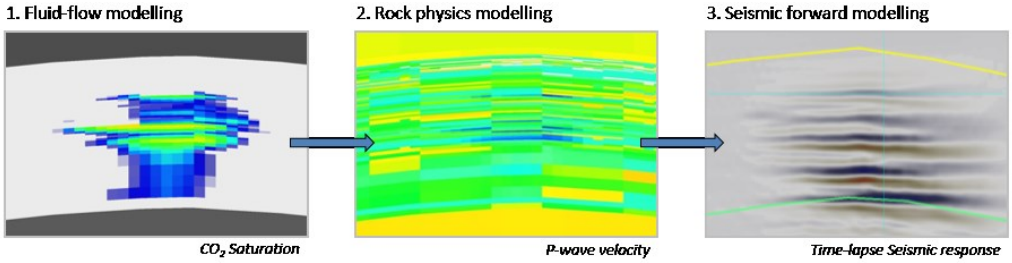

Fig. 1. Three-stage model-driven workflow used to model the time-lapse seismic response of injected CO_2.

2.1 Geological model

The model used in this study is an adaptation from Williams et al., (2013), representing part of the Triassic Bunter Sandstone Formation in the UK sector of the North Sea (Fig. 2). This formation has been identified as having the potential to store large amounts of CO_2 within the saline reservoirs (Holloway et al., 2006, Heinemann et al., 2012). The model contains 3 dip-closed structures formed by post-depositional halokinesis in the underlying halite-dominated strata of the Zechstein Group. These domes are unaffected by faulting and form ideal traps for injected CO_2. The reservoir is overlain by mudstones of the Haisborough Group, forming an effective seal.

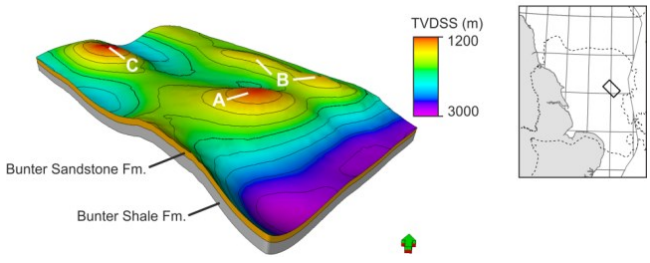

Fig. 2. Bunter Sandstone Model with each dome labelled and a location map (modified from Williams et al., 2013).

Williams et al., (2013) partitioned the formation into five zones according to changes in depositional environment interpreted from petrophysical analysis and a regional depositional model for the Bunter Sandstone. The inferred reservoir properties within the model were based on geophysical log analysis. The porosity is strongly influenced by variations in lithology, and ranges from 10% to 35% (Fig. 3). Williams et al., (2013) provide a detailed description of the reservoir model.

Each interpreted zone plays an important role in the growth and evolution of the injected CO_2. The zones provide obstacles to migration, allowing for accumulations beneath each barrier and allowing for an assessment of the potential of seismic techniques to detect them.

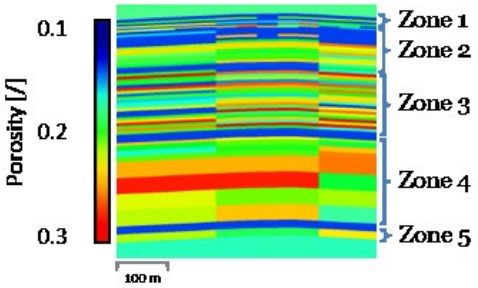

Fig. 3. Cross section through the reservoir highlighting the degree of heterogeneity in porosity.

Often, when comparing synthetic and real time-lapse seismic data for CO_2 detection or quantification, reservoirs are assumed to be homogeneous, for example in Chadwick et al., (2006) and Arts et al., (2007). If we did this here it would result in CO_2 saturations which are bi-modal in distribution with maximum saturation values equal to 1-S_{wir} (irreducible water saturation). Incorporating reservoir heterogeneity allows the range of saturations, and hence, velocity distributions to be assessed more accurately due to the tortuous migration caused by the intra-reservoir baffles. This has been demonstrated by Ghanbari et al., (2006) through the simulation of CO_2 storage in both a homogeneous and a heterogeneous model. The addition of shale layers in the model resulted in CO_2 accumulations below these baffles causing the CO_2 to flow laterally rather than vertically, distorting migration. This allows for a more accurate way to assess, understand and compare the saturation scales and phase distributions which can be expected.

For this study, we have modified the reservoir model, with a focus purely on dome A, and have included surfaces for the overburden up to the sea bed (Fig. 4). The surfaces were interpreted by PGS from their SNS MegaSurvey 3D seismic dataset (Williams et al., 2013) and were validated from existing well data and formation tops. No faults were found within the modelled area. Dome A has been chosen for this study as it provides a significant structural closure, allowing for large volumes of CO_2 to be accommodated. The top seal is also situated at an appropriate reservoir depth (1200m) for CO_2 storage. At this depth, pressures and temperatures are above the critical point, where the CO_2 is in a 'supercritical state', with the density of a liquid and the viscosity of a gas (Cook, 2012). The original model assumed all barriers within the Bunter Sandstone Formation were impermeable, with 0% porosity and 0 mD permeability. In order to allow for CO_2 plume growth and migration through these barriers up to the top seal, as well as accurate velocity calculations, we have assumed 13% porosity and 15mD permeability for all barriers in each zone. All cells with 13% porosity and 15mD permeability are assumed to be shales, while any cells with greater porosity and permeability are assumed to be sandstones. A kv/kh ratio of 0.1 was used.

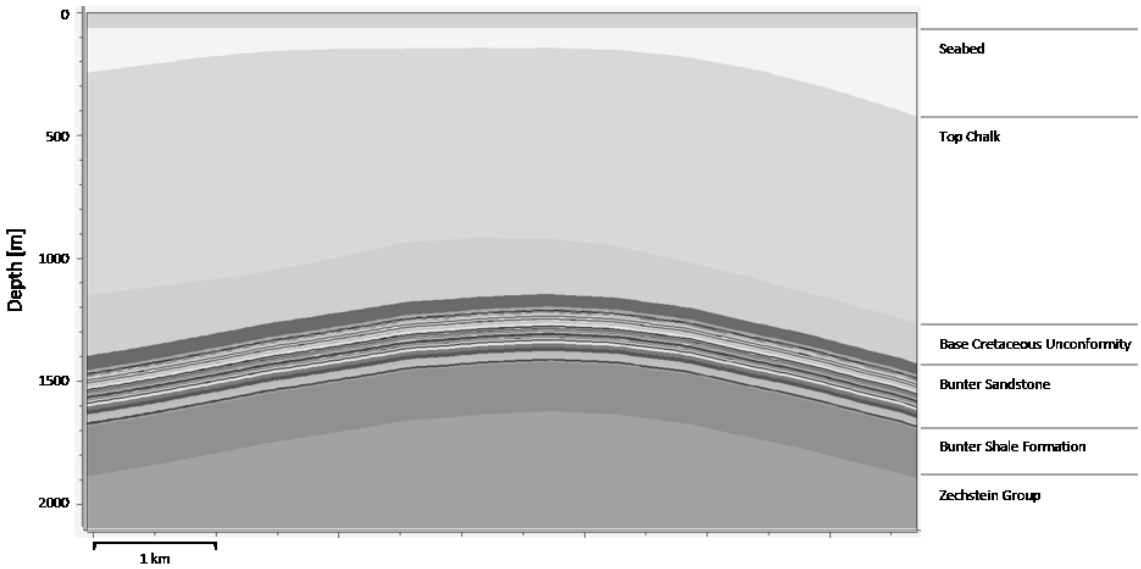

Fig. 4. Cross-section through the entire geological model with interpreted surfaces on the right-hand side (vertical exaggeration of 2). SNS MegaSurvey data courtesy of PGS.

The modified 3D model covers an area of 6750m x 4650m with horizontal cell-size dimensions of 45m x 45m throughout. Vertical cell-size within the Bunter Sandstone Formation varies from 1m to 15m depending on variations in lithology observed on the geophysical logs.

2.2 CO_2 flow modelling

Permedia's black oil simulator (Permedia, 2014) was used to simulate the migration and plume evolution of the injected CO_2 within the Bunter Sandstone, with a focus on accumulations below baffles within each zone. CO_2 injection was modelled through a single well at a constant rate of 0.1 Mt/year for 20 years through a 20m perforation interval into a high porosity sand in Zone 4 (Fig. 5). The simulation was extended for 10 years post injection to allow for continued migration and residual trapping.

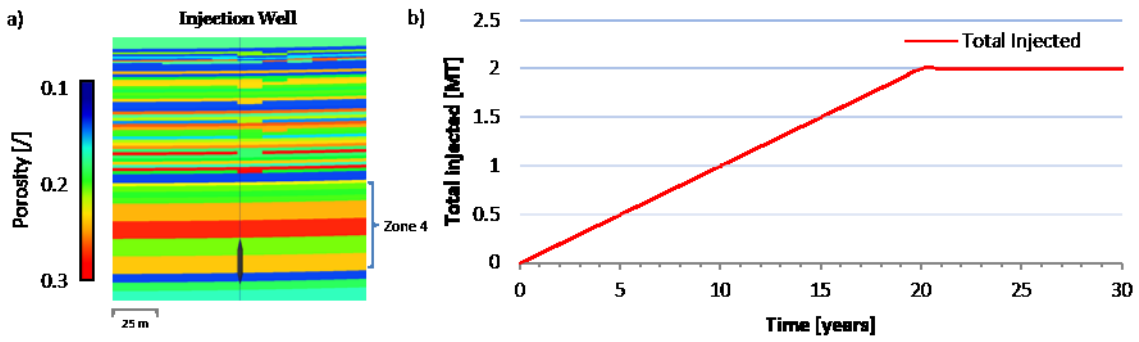

Fig. 5. a) Cross-section through the reservoir showing the injection well and 20m perforation interval (black), b) Summary of the total injected CO_2 over simulated years.

As there are no measured relative permeability or capillary pressure curves for the Bunter Sandstone, measurements from Bennion and Bachu's (2006) Cardium Sandstone were used to model drainage

and imbibition for brine and CO_2 (Fig. 6). We use the equation of state presented by Duan and Sun (2003) in this study.

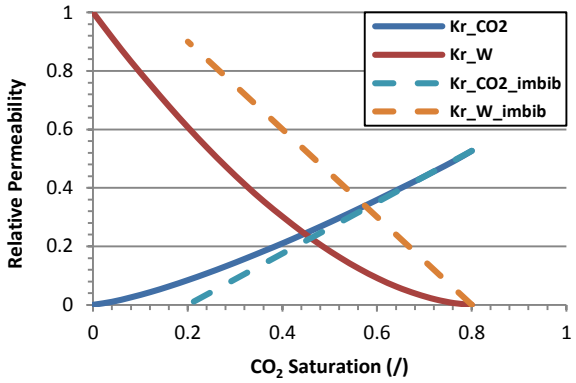

Fig 6. The two-phase relative permeability (Kr) curves used to model CO_2 flow within the reservoir. The solid lines refer to the reservoir undergoing drainage while the dashed lines represent imbibition. The curves represent an irriducable water saturation of 0.2 and residual CO_2 saturation of 0.2 (Bennion and Bachu, 2006).

2.3 Rock physics modelling

Once the water-CO_2 distributions in the reservoir have been determined, the corresponding changes in elastic properties for each simulated grid block can be calculated. We employ the Gassmann fluid substitution workflow (Smith et al., 2003).

2.3.1 Effect of fluid saturation on seismic properties

Gassmann's equation (Gassmann, 1951) is one of the most commonly used theoretical approaches for fluid substitution to estimate the effect of fluid changes on elastic properties. Gassmann's equation relates the bulk modulus of a saturated rock (K_{sat}) to its porosity (φ), pore-fluid bulk modulus (K_{fl}), matrix bulk modulus (K_m), and dry frame bulk modulus (K_{dry}) as:

$$K_{sat} = K_{dry} + \frac{\left(1-\frac{K_{dry}}{K_m}\right)^2}{\frac{\varphi}{K_{fl}} + \frac{(1-\varphi)}{K_m} - \frac{K_{dry}}{K^2 m}}. \quad (1)$$

Calculation of the saturated bulk modulus (K_{sat}) is a two-part process. It involves the calculation of the dry bulk modulus of the rock frame, drained of its initial fluid, after which the bulk modulus of the rock saturated with desired fluids is calculated (Smith et al., 2003).

The friable-sand model (Dvorkin and Nur, 1996) was used to calculate the dry frame bulk modulus (K_{dry}) and shear modulus (μ_{dry}) for the sandstone layers. This model describes the changing velocity-porosity relation with deteriorating sorting (Avseth et al., 2005). The matrix bulk modulus K_m was calculated via the application of Voigt-Reuss-Hill (VRH) averaging of the mineral constituents (Avseth et al., 2005). The constant-clay model (Avseth et al., 2005) was used to describe the velocity-porosity behaviour for shales. This model uses the same equations as for the friable-sand model, however the high-porosity end member varies as a function of the clay content. We assumed a Vclay of 90% for all shale layers in the model.

Several assumptions limit the applicability of Gassmann's equation. These have been thoroughly discussed by Berryman (1999), Smith et al., (2003), Han and Batzle (2004), Adam et al., (2006) and Dvorkin et al., (2014). One of these assumptions is that the distributed phases are immiscible and homogeneously distributed throughout the pore space (uniform fluid saturation). This assumption may be valid in homogeneous, virgin, reservoirs or trapped hydrocarbon accumulations which have come to equilibrium over long geological timescales. During drilling, production, or in this scenario - the migration of CO_2 - however, the equilibrium distribution of phases may be disturbed, resulting in a non-uniform phase distribution.

2.3.2 Fluid saturation, seismic wavelength and geological heterogeneity

The mixing of two immiscible fluids in a porous rock results in velocities that are different from those resulting from saturation with a single fluid (Domenico, 1976, Gregory, 1976). This is caused by saturation changes in the fluid bulk modulus. However, velocities depend not only on saturation, but also on the spatial distribution of the phases within the pore space (Mavko and Mukerji, 1998). When the migrating CO_2 is spatially heterogeneous, two pore-fluid distribution end-member ranges can be encountered: homogeneous, uniform fluid saturation distribution, and heterogeneous, patchy fluid saturation distribution. The varying saturations, when related to rock permeability and seismic wavelength, result in distinct velocity and reflectivity changes. The critical factor determining these ranges is the size of saturation heterogeneity, or saturation 'patch', *d*.

When the patch size exists on a scale which is very small compared with a seismic wavelength ($d \ll \lambda$), individual patches cannot be resolved, but can still influence velocity and impedance. Sub-resolution patches in this region can be divided into two states, known as relaxed and unrelaxed, dictated by hydraulic diffusivity and diffusion length (Mavko and Mukerji, 1998). These two relaxation states are related to the pore-fluid saturation end-members through the diffusion or critical length scale, L_c (m), which is given by

$$L_c = \sqrt{\frac{kK_{fl}}{f\eta}} \tag{2}$$

where f is the seismic frequency (Hz), k is the permeability (m^2) and K_{fl} and η are the bulk modulus (Pa) and viscosity (Pa-s) of the fluid respectively. The critical length scale suggests the spatial scale over which wave-induced increments of pore-pressures can reach equilibrium during a period of a seismic wave (Mavko and Mukerji, 1998). Similar expressions for the calculation of the critical diffusion length scale have been published (White, 1975, Akbar et al., 1994, Mavko and Mukerji, 1998, Knight et al., 1998, Sengupta and Mavko, 2003, Toms et al., 2006, Mavko et al., 2009, Kazemeini et al., 2010, Cairns et al., 2012).

The critical length scale for a theoretical sandstone is plotted versus frequency in Fig. 7. The curve represents both the length scales over which fluid phases interconnect, and the resultant relaxation state in the reservoir. For a given frequency, a relaxed, uniform saturation distribution is assumed at a scale less than the calculated critical length scale, while unrelaxed, patchy saturations occur at a coarser scale, greater than the critical length scale. Both saturation scales are specific to sub-seismic scale resolution, where $L_c \ll \lambda$. Assuming a P-wave velocity of 3000 m/s, a frequency of 50 Hz has a seismic wavelength of 60m ($\lambda = v/f$), whereas the critical length scale is 0.2m at the same frequency.

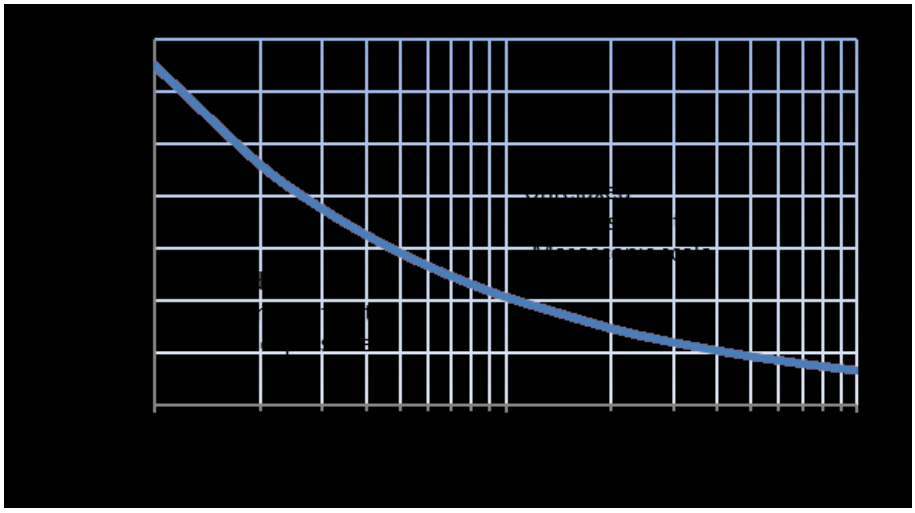

Fig. 7. Critical length scale versus frequency for a patch saturated with CO_2 with a bulk modulus of 0.0993 GPa, viscosity of 0.58 cP and permeability of 9.87E-13 m^2. These values represent CO_2 in a supercritical state, at temperature and pressure conditions of 50 °C and 15.5 MPa, respectively.

Uniform saturation refers to a scale of heterogeneity which is smaller than the critical length scale L_c and the seismic wavelength ($d < L_c << \lambda$). At this scale, wave-induced pressure oscillations between the different fluid phases have sufficient time to flow and relax, reaching a local isostress during a seismic period (Sengupta and Mavko, 2003). At these low frequencies, there is enough time for fluids to flow between gas- and liquid-filled areas, resulting in a less stiff porous rock which in turn results in lower wave velocities (Toms et al., 2006). This equilibration of pore pressure allows for the assumption of a homogeneously saturated region, where the replacement of mixed fluid phases with an effective fluid bulk modulus can be applied (Domenico, 1976). This can be determined through the application of the Reuss average (Reuss, 1929):

$$K_{fl} = \left(\frac{S_{CO_2}}{K_{CO_2}} + \frac{S_{brine}}{K_{brine}}\right)^{-1} \quad (3)$$

where S is the saturation and K is the bulk modulus of the subscript indicated fluids.

Examples of fluids distributed at this scale include irreducible water saturation (the portion of the pore volume occupied by water in a water-wet reservoir at maximum hydrocarbon saturation) and CO_2 ganglia (isolated blobs of CO_2 occupying only one to several pores formed by detachment from the larger plume body (Niven, 2006)).

When fluid heterogeneities exist on a scale greater than the critical length scale but less than wavelength scale ($d > L_c << \lambda$), there is not enough time during a seismic period for wave-induced pore pressure equilibration. Fluid heterogeneities at this scale result in spatially varying distributions, which arise due to variations in porosity, permeability, wettability and grain types. As the patch size is larger than the critical diffusion length scale, there is not enough time for pressure equilibration during a seismic period, resulting in patches of rock which remain at different pressures. As a result, it is no longer valid to use an effective fluid bulk modulus calculated using the Reuss average. In this case, the effective rock stiffness of the rock is in an 'unrelaxed state' and can be estimated using Hills (1963) constant shear modulus equation:

$$K_{fl} = \left(\frac{S_{co_2}}{K_{co_2}+(4/3)\mu_{sat}} + \frac{S_{brine}}{K_{brine}+(4/3)\mu_{sat}}\right)^{-1} - \frac{4}{3}\mu_{sat} \quad (4)$$

where K_{co_2} and K_{brine} are the bulk moduli of the rock saturated with CO_2 and brine, respectively. If the dry frame bulk modulus (K_{dry}) of the rock is elastically homogeneous, the shear modulus of the saturated rock is equal to the shear modulus of the dry rock because it is not affected by pore fluids and therefore remains unchanged during fluid substitution, therefore, $\mu_{sat} = \mu_{dry}$ (Dvorkin and Nur, 1998, Kazemeini et al., 2010).

Calculating the fluid bulk modulus using Hills's (1963) equation produces saturation ranges from 0 to 100%. In reality, the range of saturations within a pore space is constrained by limits for irreducible water saturation (S_{wir}) and residual saturation (R_{CO2}). This means that CO_2 saturation cannot exist at $S_{CO2} > 1\text{-}S_{wir}$, where deviation of the patchy curve starts at a given irreducible water saturation.

Following Sengupta and Mavko (2003) and Cairns et al., (2012), the effective brine (S'_{brine}) and CO_2 (S'_{CO_2}) saturations resulting from the lower limit placed due to S_{wir} can be calculated as:

$$S'_{brine} = \frac{S_{brine}-S_{wir}}{1-S_{wir}} \quad (5)$$

$$S'_{CO_2} = \frac{S_{CO2}}{1-S_{wir}} \quad (6)$$

The modified bulk modulus of CO_2 ($K'_{sat\ CO_2}$), which is either completely brine-filled or a mix of CO_2 and residual brine can be calculated as:

$$K'_{sat\ CO_2} = \left(\frac{S_{wir}}{K_{sat\ brine}} + \frac{1-S_{wir}}{K_{sat\ co_2}}\right)^{-1} \quad (7)$$

Following this, the modified Hill average during the injection of CO_2 then becomes:

$$K_{fl} = \left(\frac{S'_{CO_2}}{K'_{sat\ co_2}+(4/3)\mu_{sat}} + \frac{S'_{brine}}{K_{sat\ brine}+(4/3)\mu_{sat}}\right)^{-1} - \frac{4}{3}\mu_{sat} \quad (8)$$

Patchy unrelaxed states result in high induced pressures and an increase in material stiffness which consequently lead to higher velocities. For this reason, patchy saturation represents the upper bound of seismic velocities as a function of saturation at seismic frequencies (Sengupta and Mavko, 2003, Cairns et al., 2012). Furthermore, Johnson (2001) and Mavko and Mukerji (1998) have both shown that mesoscopic-scale (patchy) fluid distributions lead to a stiffer rock, and consequently higher velocities than those arising from microscopic-scale (uniform) distributions, and that these represent the upper and lower bounds of fluid bulk modulus.

2.3.3 Sensitivity to fluid saturation model

Fig. 8 shows the possible range in values for P-wave velocity (V_p) predicted using the three saturation models; patchy, modified-patchy and uniform saturation. The results show that the change in V_p, as a function of CO_2 saturation, is heavily dependent on the saturation model used to calculate the elastic properties. These results are similar to those obtained by Sengupta and Mavko (2003), Toms et al., (2006), Lumley (2010), and Cairns et al., (2012).

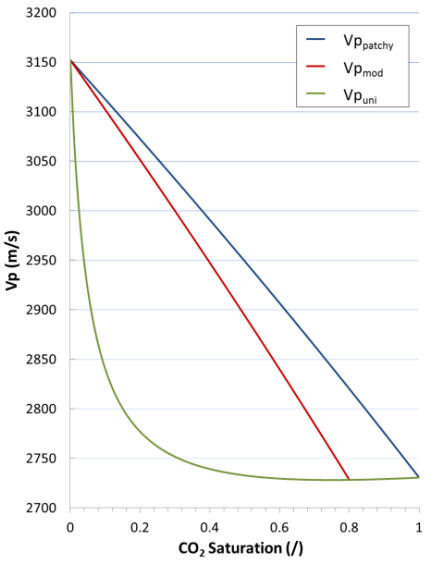

Fig. 8. P-wave velocity (Vp) as a function of CO_2 saturation calculated assuming a Gassmann-Reuss, uniform saturation model (Vp_{uni}), Gassmann-Hill patchy model, assuming no irreducible water saturation (Vp_{patchy}), and the modified Gassmann-Hill model assuming an irreducible water saturation of 20% (Vp_{mod}).

The Gassmann-Reuss (uniform saturation) model predicts a rapid change of about -12% in V_p as CO_2 saturation increases from 0 to ~20%, while showing very little further change at higher saturations. However, patchy and modified patchy models predict a linear V_p-saturation relationship showing a linear decrease in velocity with increasing saturation. The large range of possible saturations for a given velocity demonstrates the importance of understanding and modelling the range of fluid saturation distribution models (uniform/patchy) when predicting the fluid bulk modulus prior to generating and interpreting the seismic response. Furthermore, the large range of saturations has great implications for CO_2 quantification from seismic velocities as it highlights the level of uncertainty which could be encountered. This is evident in Fig. 8, where an observed change in velocity of -300 m/s could result from either 12% CO_2 assuming a uniform saturation distribution or 60% CO_2 assuming a patchy saturation distribution. Assuming purely a uniform saturation distribution could potentially underestimate the amount of stored CO_2 in the subsurface.

Furthermore, the water-CO_2 distributions from the CO_2 flow modelling results represent a single 'homogeneous' saturation value for each grid cell. Each value is then used to compute velocity, where a choice of two models are available – modified patchy and uniform – depending on the critical length scale and the size of the fluid patches. As cell dimensions are typically chosen to optimize flow modelling, reservoir models are built with coarse grid-cells, as evident with the Bunter model, which has vertical cell-size dimensions of 1 – 15m. Cell size dimensions at these scales are much greater than the calculated critical length scales for the range of seismic frequencies shown in Fig. 7. This indicates that the saturation distribution within each grid cell is not clearly modelled. To account for this, we assume that each cell with a single 'homogeneous' saturation value represents the bulk saturation of the cell, whereas in fact each cell will, in theory, have varying saturations of CO_2 at the meso-scale. As we are dealing with sub-seismic scale saturation distributions, we feel that this assumption is valid as saturations distributed at this scale are not resolvable on seismic but still influence seismic velocity and impedance.

It should also be noted that the calculation of the end-member models assumes a single rock facies with homogeneous lithology such that K_m, K_{dry} and φ are uniform in space. Spatial variations in velocities are assumed to result only from differing pore fluid saturations (Mavko and Mukerji, 1998). This is not valid for all reservoir conditions, particularly for modelling heterogeneous reservoirs with spatially varying properties such as porosity and permeability. Heterogeneous reservoirs would result in a range of velocities distributed between the patchy and uniform saturation end-member models determined by variations in permeability, fluid viscosity, and patch size (Mavko and Mukerji, 1998, Sengupta and Mavko, 2003, Lebedev et al., 2009, Cairns et al., 2012). Furthermore, the flow of CO_2 through a volume in the subsurface would result in a transition from patchy to uniform saturation distribution with increasing time. This transition has been demonstrated by Lebedev et al., (2009) in laboratory experiments, where the authors suggest that it occurs as a result of the interplay between the characteristic size and distribution of the fluid patches and the diffusion length, controlled by properties of the rock matrix, pore fluids and signal frequency. Understanding the rate at which this transition occurs, and at what patch size and overall saturation, is still an area of research which needs to be addressed.

Although we have not addressed the reasoning behind this transition in this study, we have accounted for it by simulating the end member models – uniform and modified-patchy – for each time-step in order to generate the widest range of velocities which could be encountered.

2.4 Seismic forward modelling

Using Nucleus+ (Taylor and Julliard, 2013), 2D elastic finite-difference wave propagation modelling was applied to simulate the acquisition of a single line towed streamer seismic survey based on acquisition parameters similar to real time-lapse data (Table 1). The source signature is a zero-phase Butterworth wavelet of 2.0 msec sample interval, with low cut and high cut frequencies of 8Hz and 90Hz and slopes of 18 and 72 dB/octave, respectively (Fig. 9).

Synthetic shot records were generated along a 6km east-west section. The modelling was performed for selected monitoring stages, for both uniform and modified-patchy saturation cases. After NMO correction, the traces were stacked and depth migrated using the phase-shift plus interpolation (PSPI) method (Ferguson and Margrave, 2005), available through the CREWES toolkit in Matlab (Margrave, 2003).

Table 1: Synthetic seismic modelling acquisition parameters

Acquisition parameters	
Receiver spacing	25 m
Source spacing	25 m
Cable length	5500 m
Number of receivers	236
Number of shots	220
Recording length	2 sec

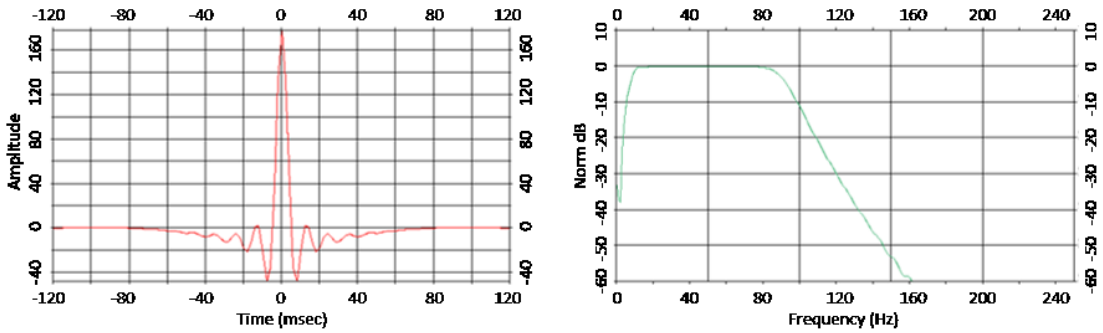

Fig. 9. Zero-phase Butterworth wavelet at 2.0 msec sample interval. A low and high cut frequency of 8 and 90Hz and low and high cut slope of 18 and 72 db/octave were applied.

3. Results

3.1 CO_2 saturation distribution

Fig. 10(a-c) shows 2D sections of the 3D simulation results at three stages (5 years, 11 years and 20 years) of plume evolution within the reservoir. Figure 10(d-f) shows the histogram of saturations within the grid blocks. After 5 years and 0.5MT of injected CO_2, the plume has accumulated below two intra-formational baffles within Zone 4 with a mean and maximum saturation of 17% and 50%, respectively. After 11 years of injection, the plume has breached the baffle at the top of Zone 4 and has penetrated into Zone 3 while also growing laterally (Fig. 10b). Increasing CO_2 concentrations below the baffles in Zone 4 are shown at an average of 20%, with maximum saturations of 55%. A migrating leg west of the plume is also evident due to increased lateral migration reaching an area with no sealing lithology. After 20 years of injection, CO_2 breaches the baffle at the top of Zone 3 and penetrates into Zone 2, resulting in a free-phase migrating front of dimensions 271m by 30 m. Saturations in the reservoir as a whole are shown at an average of 23%, with maximum saturations of 62%. The saturation of the CO_2 is shown to be very heterogeneous due to the heterogeneous nature of the reservoir.

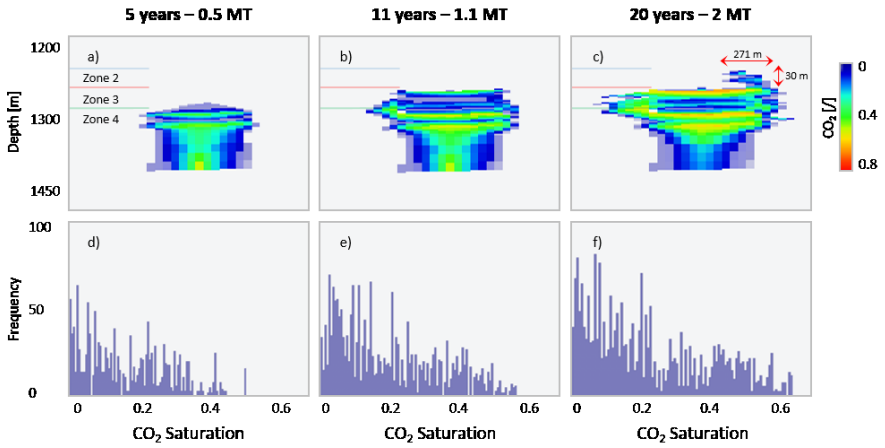

Fig. 10. 2D sections of the 3D simulation highlighting three stages of plume evolution, and histograms showing the associated ranges in saturations within the Bunter Sandstone reservoir; after 5, 11 and 20 simulated years. Vertical exaggeration of 3.

3.2 Heterogeneous reservoir velocity distribution

The heterogeneous nature of the Bunter Sandstone reservoir results in a distribution of velocities which range from 1800 m/s to 3500 m/s, depending on lithology, porosity and fluid saturation (Fig. 11). These ranges match typical velocities for shales and saturated sandstones (Bourbié et al., 1987) and are dependent on porosity and fluid saturation.

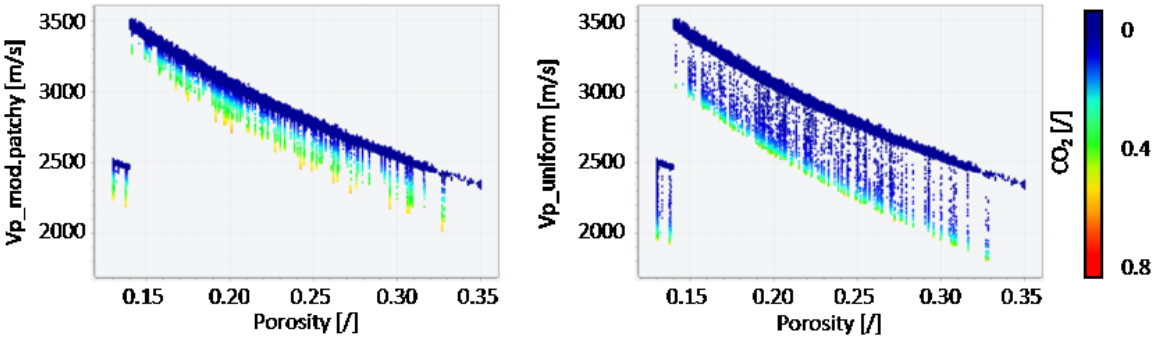

Fig. 11. Calculated velocity as a function of porosity for the Bunter Sandstone, coloured by CO_2 saturation. Velocity is calculated assuming both a modified patchy (left) and uniform saturation model (right). Calculated velocities less than 14% correspond to shale layers within the model.

The calculated velocities for the Bunter Sandstone reservoir show an approximately linear relationship between velocity and porosity, as expected. An increase in CO_2 saturation of 80% shows a maximum decrease in velocity from -350 to -550 m/s depending on the velocity model used. The saturation change highlights the key differences between uniform and modified-patchy saturation, where patchy saturation results in a linear change in velocity with increasing fluid content, the uniform saturation results in a sharp decrease in velocity at low saturations, with minimal to no change thereafter.

Fig. 12(a-l) represents the calculated velocity models assuming both modified-patchy and uniform saturation for each stage of CO_2 plume evolution. Analysis of the change in velocity with the baseline clearly highlights the differences between the two models. A focus on the uniform velocity modelling results (Fig. 12g-l) shows that the change in velocity is as great as -550 m/s from the outset, with a very minimal change in velocity of only -5 m/s within the plume body when comparing each stage. Large changes in velocity are evident throughout each stage allowing for clear distinction between the CO_2 plume and the reservoir. However, features within the plume itself, such as the immobile CO_2 accumulations below intra-formational baffles, are difficult to distinguish from the plume. The velocity model calculated assuming a modified-patchy saturation model (Fig. 12a-f) highlights the main differences between the two models as it allows features within the plume body to be distinguished. A maximum velocity change of only -220 m/s is evident after 5 years. With increasing accumulations below the intra-reservoir baffles, the change in velocity is shown to be as great as -270 m/s after 11 years and -450 m/s after 20 years. This change in velocity is similar to those calculated assuming a uniform saturation distribution. At these high saturations, the magnitude of the velocity change is independent of the model used as the calculated velocities converge as the maximum saturation is reached. A focus on the free-phase migrating front of CO_2 within Zone 2 after 20 years shows a change of velocity of roughly -110 m/s for the patchy model and -400 m/s for the uniform model.

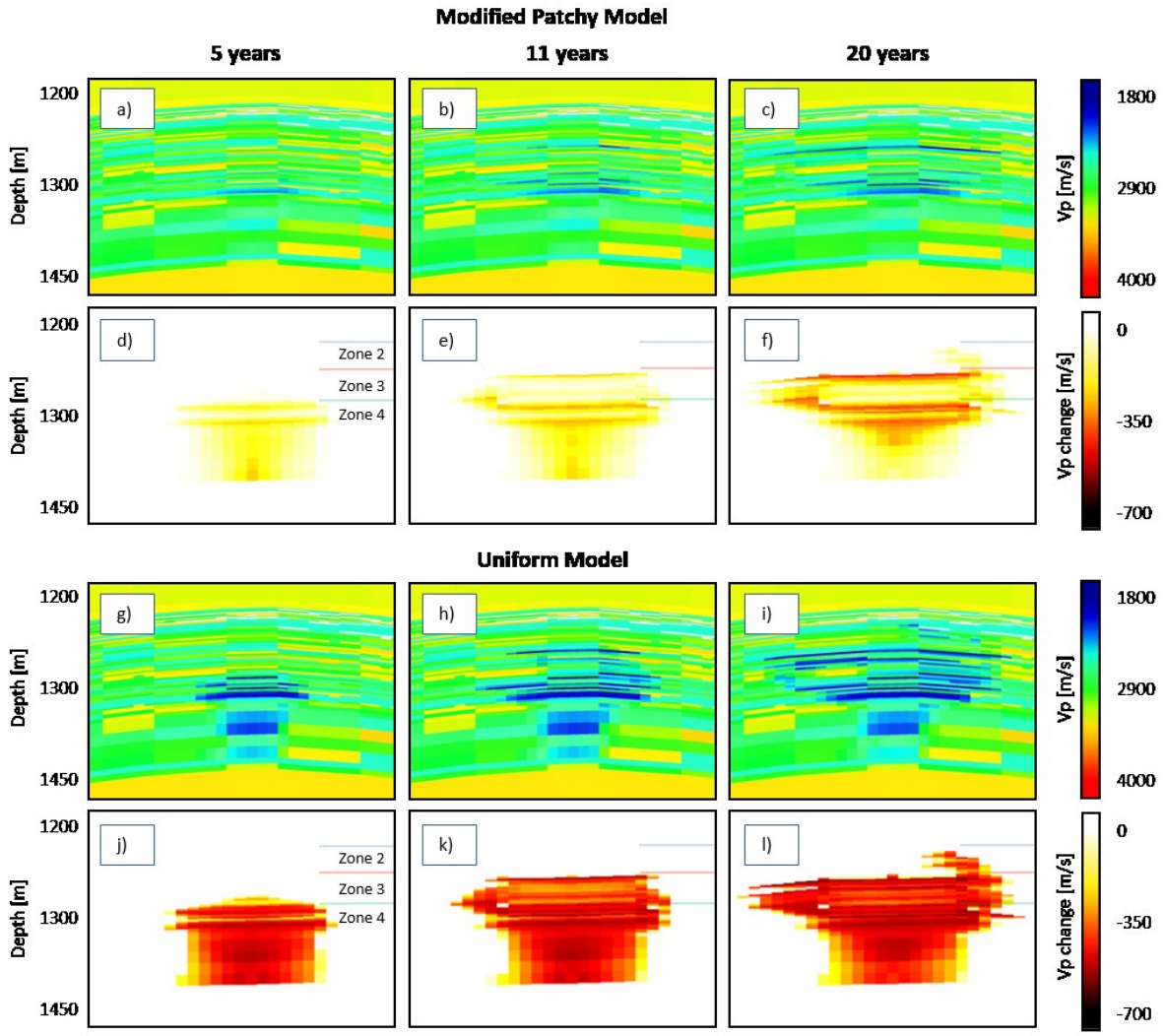

Fig. 12. Results highlighting the petrophysical modelling results. (a-c) show the calculated V_p assuming a modified-patchy model, (d-f) highlighting the change with V_p, (g-i) calculated V_p assuming a uniform saturation model, (m-o) highlighting the change in V_p with baseline. The coloured line represent the locations of the three interpreted zones within the reservoir. Vertical exaggeration of 3.

3.3 Time-lapse seismic response

The depth-migrated seismic section, juxtaposed with the velocity model, is shown in Fig. 13. Strong amplitude reflections are clearly evident at interfaces where the seismic velocity changes abruptly. Within the Bunter reservoir, reflectivity is increased due to increased heterogeneity, producing lateral changes in velocity. High amplitude reflectors within the reservoir correspond to the low porosity sands.

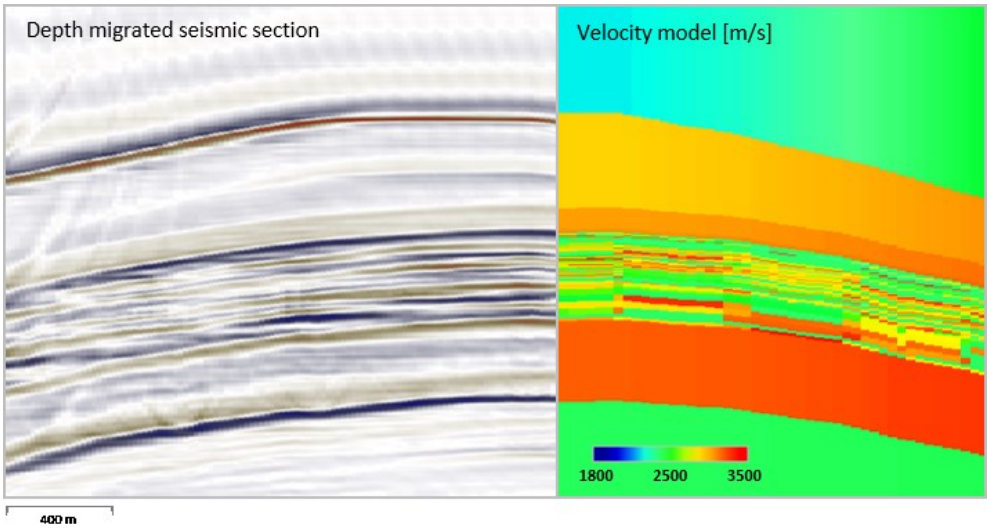

Fig. 13. Depth migrated seismic section (left), juxtaposed with the velocity model (right) for comparison. Vertical exaggeration of 2.

The introduction of CO_2 into the reservoir results in an increase in reflectivity and a prominent time-shift. The time-lapse sections (Fig. 14d-i) show clear differences between the uniform and modified-patchy saturation models. The synthetic seismic results calculated using the uniform velocity model show a clear change in amplitude, as well as a prominent time-shift below the plume. The synthetics calculated using the modified-patchy model are very different, with lower amplitude reflectors, often corresponding to zones of highly saturated, structurally trapped CO_2.

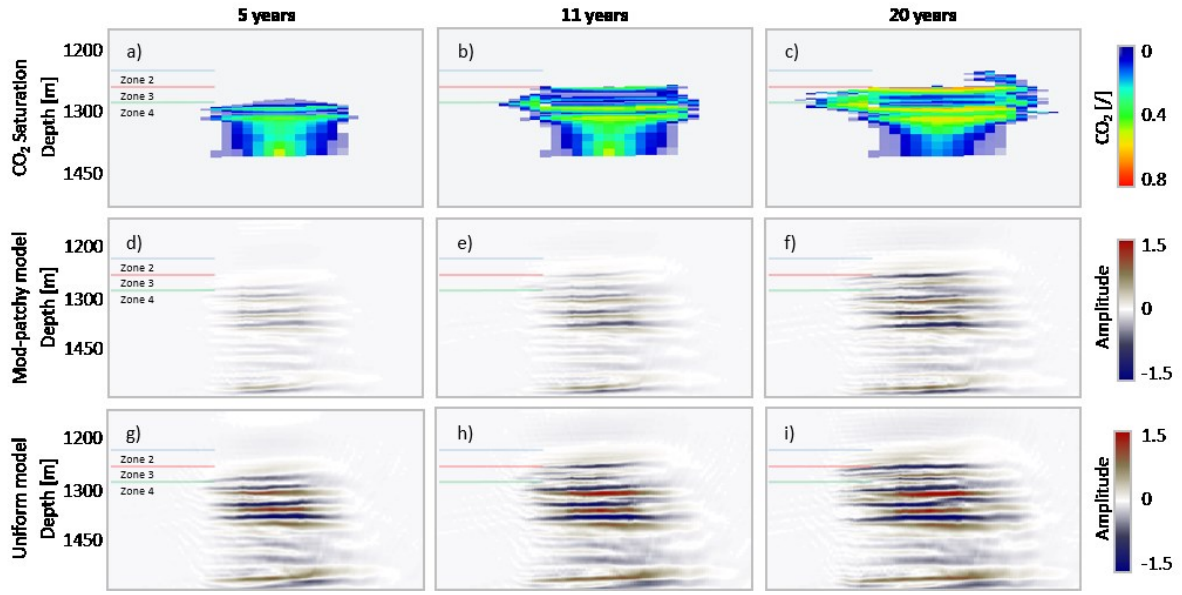

Fig. 14. Time-lapse synthetic seismic sections calculated using the modified-patchy and uniform velocity models for each stage in plume growth. The coloured lines represent the locations of the three interpreted zones within the reservoir. Vertical exaggeration of 3.

4. Discussion

4.1 Monitorability of plume growth within a reservoir

A comparison of the three modelled stages provides confidence in the ability of seismic techniques to image plume growth and evolution within the reservoir, as the top-most reflector in each seismic section corresponds to the top-most accumulation of CO_2.

Furthermore, a detailed look at the plume after 20 years (Fig. 15) shows negative seismic impedance contrasts corresponding to the structurally trapped CO_2. Interpretation of the modified-patchy model shows three primary reflectors, which can be attributed to the three main CO_2 accumulations. The amplitude of the reflector is also shown to be strongest at the centre, gradually becoming weaker farther out in both directions, as highlighted in the enlarged box in Fig. 15. Although this can also be interpreted in the uniform seismic section, it proves more difficult as each reflector shows a large change in amplitude throughout. As the subtle change in amplitude is directly related to the concentration of CO_2 within each accumulation, it suggests that patchy saturation has important implications for the detection of CO_2 movement and for the quantification of volume of CO_2 injected into the reservoir. Previously, when quantifying the total amount of injected CO_2, a uniform saturation distribution has been assumed (for example, Chadwick et al., 2005). Through 4D seismic quantification, Chadwick et al., (2005) were able to account for 85% of the total amount of injected CO_2 in the Utsira Formation. By assuming a patchy saturation distribution, a more appropriate account for the injected CO_2 might be possible. However, this is an issue of non-uniqueness due to the transition from patchy to uniform saturation with increasing time.

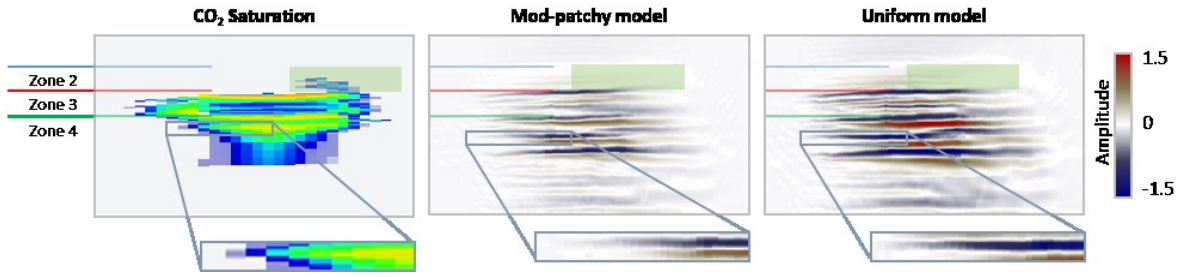

Fig. 15. Detailed look at the simulated CO_2 plume after 20 years. The location of each reservoir zone is shown as well as the location of the free-phase migrating CO_2 front, highlighted in the olive green box. The enlarged box highlights the change in amplitude corresponding to the accumulation of CO_2 in Zone 4.

A focus on the free-phase migrating front of CO_2 in Zone 2, highlighted by the olive green box in Fig. 15, shows very little change in amplitude in the synthetic seismic sections for both the modified-patchy and uniform models. This shows that a migrating front of CO_2 appears to be difficult to detect. However, it should be noted that the estimated saturations within the CO_2 plume, and of the migrating front in particular, play a key role when assessing detectability, namely through the relative permeability and capillary pressure functions entered into the reservoir simulator. Therefore this is a site-specific issue, where different curves may predict a greater range of CO_2 saturation, to which the change in velocity is particularly sensitive.

4.2 Implications for the detection of a migrating front

The ability to detect CO_2 migration within a reservoir is critical to the successful demonstration of containment. The detection of movement within the reservoir, in particular if outside the primary storage reservoir or storage complex, could provide operators with an early warning system, should a loss of containment occur.

Interestingly, results from the modelling undertaken in this study, when focused on the detection of a migrating front of CO_2, show that neither the modified-patchy nor the uniform models results in an interpretable change in amplitude. This highlights the fact that the detection of a free-phase migrating front of CO_2 is predominantly dependent on its spatial geometry. Once the size of the front crosses a particular detectability threshold, the pore-fluid saturation distribution models - patchy or uniform – will play an important role.

To test the importance of spatial geometry on the detection of a migrating front of CO_2, we applied the same workflow to a further stage in the simulation - after 30 years - and compared the modelled results with the results after 20 years. When focused on the migrating front alone (Fig. 16) the models show that the front has increased in size - from 271m to 584m (Fig. 16a-b) - as well as in saturation - from an average of 10% to 20% CO_2 (Fig. 16c-d). This results in a maximum calculated change in velocity from -135 to -297 m/s assuming a modified-patchy distribution and -466 to -527 m/s assuming a uniform distribution (Fig. 16e-h).

A comparison of the generated synthetic seismic sections shows a clear interpretable amplitude change within Zone 2 when assuming a uniform distribution after 30 simulated years (Fig. 17f). The modified-patchy results also show a change in amplitude at this time, although this is less obvious (Fig. 17e). This provides confidence in the ability of seismic techniques to detect a migrating front only when a particular threshold in the lateral size of the plume has been reached. We should emphasize the point that these synthetics represent noise-free time-lapse responses. It is always possible of course that the presence of noise could result in the migrating front becoming undetectable.

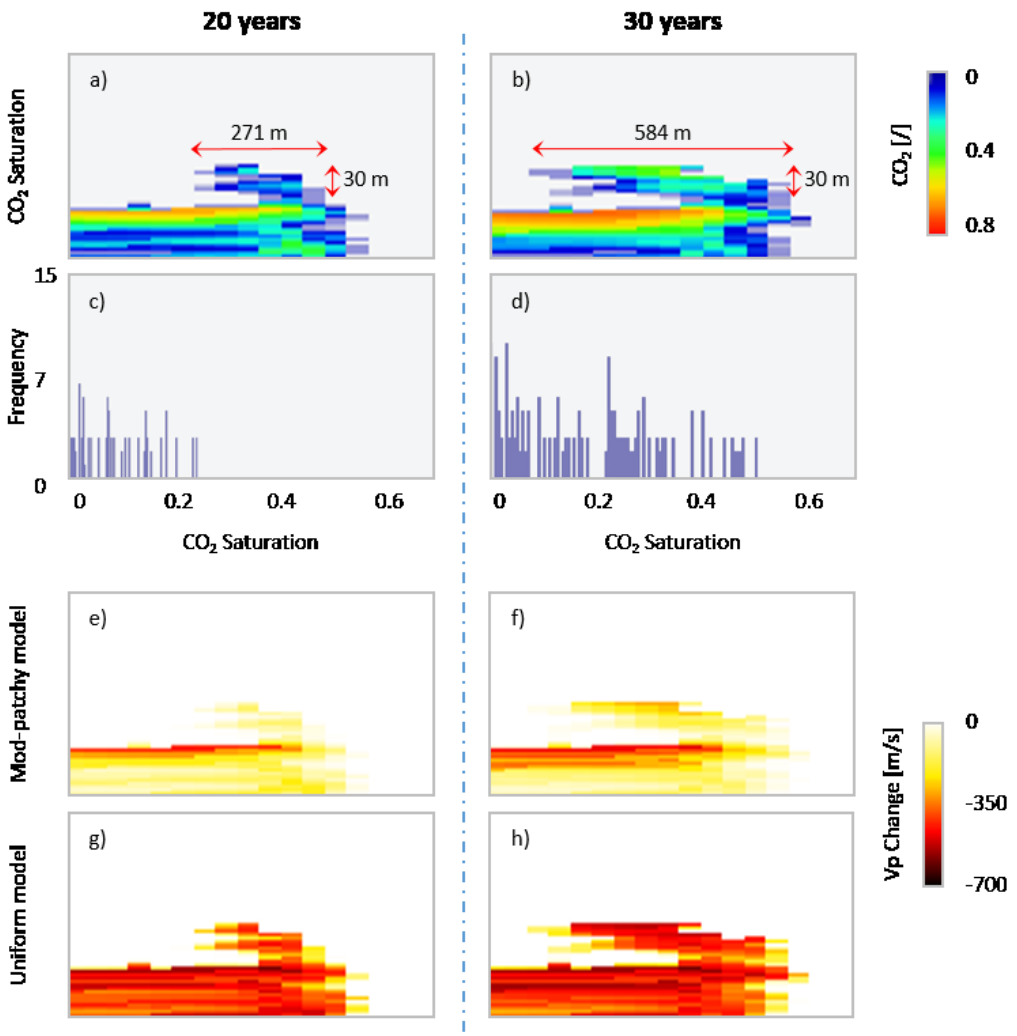

Fig. 16. Comparison of the simulated results after 20 and 30 simulated years. (a-d) highlight the change in lateral distribution and CO_2 saturation of the migrating front while (e-h) highlight the change in velocity assuming both a modified-patchy and uniform saturation distribution. Vertical exaggeration of 3.

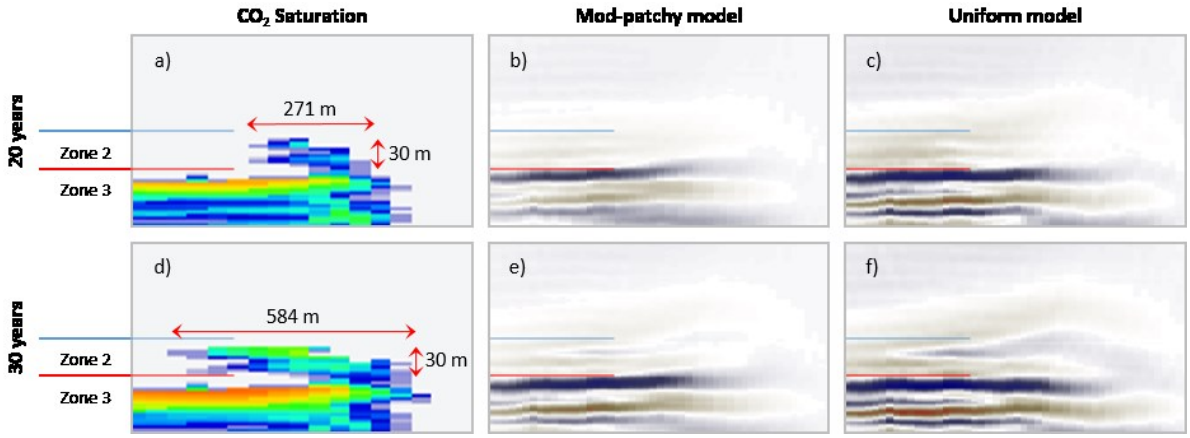

Fig. 17. Comparison of the seismic time-lapse modelling of the migrating front after 20 (a-c) and 30 (d-f) simulated years assuming both a modified-patchy (b and e) and uniform distribution (c and f). Vertical exaggeration of 3.

5. Conclusions

The key contribution of this study is to account for, and understand, the saturation scales and the phase distributions within the reservoir which could be encountered, therefore affecting the velocity changes resulting from the injected CO_2. Through the application of a three-stage model-driven workflow, we have modelled two end-member fluid distribution models, uniform and modified-patchy, to generate the widest range of velocity distributions for each chosen time-step. This has been done to account for the transition from patchy to uniform saturation distribution with increasing CO_2 in order to assess the potential of seismic monitoring techniques to image the plume growth, evolution, and migration of injected CO_2 in the subsurface.

The presence of reservoir heterogeneity added another layer of complexity to both the CO_2 flow and rock physics modelling as it resulted in a range of CO_2 saturations and distribution of velocities. Traditionally, simulated CO_2 flow modelling using a homogeneous model would result in saturations which are either structurally trapped (immobile) or mobile. This would result in CO_2 concentrations which are 'uniform' in accumulation, with maximum saturation values of $1\text{-}S_{wir}$. Rock physics modelling applied to such a model would result in velocities which are very similar for patchy and uniform cases as both curves converge at high saturations (as shown in Fig. 8). For such a scenario, velocities calculated assuming either a patchy or a uniform model would not matter as they would return similar values. The addition of reservoir heterogeneity corrected for this as it resulted in a range of saturations within the reservoir due to the tortuous migration from the intra-reservoir baffles, allowing for a more accurate way to assess, understand and compare the saturation scales and the phase distributions which could be expected.

Through the application of a heterogeneous model, the generated synthetic seismic sections show clear differences between the modified-patchy and uniform saturation models. In both cases the CO_2 growth within each zone can be detected, where the top-most reflector corresponds to the top-most accumulation in the simulation. Furthermore, each accumulation of CO_2 below the intra-formational baffles in each zone can be interpreted regardless of the assumed fluid saturation model. This provides confidence in the ability of seismic methods to detect plume growth and evolution within a saline reservoir.

A comparison of the modified-patchy and uniform synthetic seismic sections shows a clear difference in amplitude and time-shift. Although the uniform model shows high changes in amplitude and large velocity push-down effects below the plume, it proves difficult to distinguish the different CO_2 accumulations within each zone. The modified-patchy model results in a more subtle change in amplitude. As the subtle change in amplitude is directly related to the concentration of CO_2 within each accumulation, it suggests that this difference has important implications for CO_2 detectability and for quantifying the volume of CO_2 injected into the reservoir.

A free-phase migrating front of CO_2 was shown to be more difficult to detect as the ability to image this is dependent not only on the fluid saturation distribution, but also on the spatial geometry of the front. It required an increase in lateral size for the front to become detectable. This provides confidence in the ability of seismic techniques to detect a migrating front only when a particular threshold in plume-geometry has been reached. This however was imaged through noise-free synthetic time-lapse responses. It is possible that the presence of noise could result in the migrating front becoming undetectable.

Finally, it should be noted that the saturation and distribution of the CO_2 in this study play a key role when assessing detectability, namely through the relative permeability and capillary pressure functions entered into the reservoir simulator. This is a site-specific issue, where different curves may predict different ranges of CO_2 saturation, to which the changes in velocity are particularly sensitive. Assessing these site-specific variations, through the application of the workflow presented in this study, during initial storage-site assessment stages, could provide valuable information regarding the ability to image CO_2 plume growth, and importantly, migration.

Acknowledgements

The authors thank E.ON and Energy Technology Partnership (ETP) for sponsoring this work, and Petroleum Geo-Services (PGS) and British Geological Survey (BGS) for allowing the use and publication of the Bunter model. We also thank Silke Bude at PGS for her great help and guidance in using Nucleus+. We are also grateful for CREWES for allowing the use of their seismic modelling software.

References

ADAM, L., BATZLE, M. & BREVIK, I. 2006. Gassmann's fluid substitution and shear modulus variability in carbonates at laboratory seismic and ultrasonic frequencies. *Geophysics,* 71**,** F173-F183.

AKBAR, N., MAVKO, G., NUR, A. & DVORKIN, J. 1994. Seismic signatures of reservoir transport properties and pore fluid distribution. *Geophysics,* 59**,** 1222-1236.

ARTS, R., CHADWICK, A., EIKEN, O., THIBEAU, S. & NOONER, S. 2008. Ten years' experience of monitoring CO2 injection in the Utsira Sand at Sleipner, offshore Norway. *First break,* 26.

ARTS, R., CHADWICK, R., EIKEN, O., TRANI, M. & DORTLAND, S. Year. Synthetic versus real time-lapse seismic data at the Sleipner CO2 injection site. *In:* 2007 SEG Annual Meeting, 2007 2007. Society of Exploration Geophysicists.

ARTS, R., EIKEN, O., CHADWICK, A., ZWEIGEL, P., VAN DER MEER, L. & ZINSZNER, B. 2004. Monitoring of CO2 injected at Sleipner using time-lapse seismic data. *Energy,* 29**,** 1383-1392.

AVSETH, P., MUKERJI, T. & MAVKO, G. 2005. Quantitative seismic interpretation. *Quantitative Seismic Interpretation, by Per Avseth and Tapan Mukerji and Gary Mavko, pp. 376. ISBN 0521816017. Cambridge, UK: Cambridge University Press, March 2005.,* 1.

BENNION, D. & BACHU, S. Year. Dependence on temperature, pressure, and salinity of the IFT and relative permeability displacement characteristics of CO2 injected in deep saline aquifers. *In:* SPE Annual Technical Conference and Exhibition, 2006.

BERGMANN, P., YANG, C., LÜTH, S., JUHLIN, C. & COSMA, C. 2011. Time-lapse processing of 2D seismic profiles with testing of static correction methods at the CO2 injection site Ketzin (Germany). *Journal of Applied Geophysics,* 75**,** 124-139.

BERRYMAN, J. G. 1999. Origin of Gassmann's equations. *Geophysics,* 64**,** 1627-1629.

BOAIT, F. C., WHITE, N. J., BICKLE, M. J., CHADWICK, R. A., NEUFELD, J. A. & HUPPERT, H. E. 2012. Spatial and temporal evolution of injected CO2 at the Sleipner Field, North Sea. *Journal of Geophysical Research: Solid Earth,* 117**,** n/a-n/a.

BOURBIÉ, T., COUSSY, O. & ZINSZNER, B. 1987. Acoustics of porous media: Editions Technip. *Paris, France*.

CAIRNS, G., JAKUBOWICZ, H., LONERGAN, L. & MUGGERIDGE, A. 2012. Using time-lapse seismic monitoring to identify trapping mechanisms during CO2 sequestration. *International Journal of Greenhouse Gas Control,* 11**,** 316-325.

CHADWICK, A., ARTS, R., EIKEN, O., WILLIAMSON, P. & WILLIAMS, G. 2006. Geophysical monitoring of the CO2 plume at Sleipner, North Sea. *Advances in the geological storage of carbon dioxide*, 303-314.

COOK, P. 2012. *Clean energy, climate and carbon*, CSIRO PUBLISHING.

DOMENICO, S. 1976. Effect of brine-gas mixture on velocity in an unconsolidated sand reservoir. *Geophysics,* 41, 882-894.

DUAN, Z. & SUN, R. 2003. An improved model calculating CO2 solubility in pure water and aqueous NaCl solutions from 273 to 533 K and from 0 to 2000 bar. *Chemical Geology,* 193, 257-271.

DVORKIN, J., GUTIERREZ, M. A. & GRANA, D. 2014. *Seismic reflections of rock properties*, Cambridge University Press.

DVORKIN, J. & NUR, A. 1996. Elasticity of high-porosity sandstones: Theory for two North Sea data sets. *Geophysics,* 61, 1363-1370.

DVORKIN, J. & NUR, A. 1998. Acoustic signatures of patchy saturation. *International Journal of Solids and Structures,* 35, 4803-4810.

FERGUSON, R. J. & MARGRAVE, G. F. 2005. Planned seismic imaging using explicit one-way operators. *Geophysics,* 70, S101-S109.

GASSMANN, F. 1951. *Über die elastizität poröser medien*, Inst. für Geophysik an der ETH.

GHANBARI, S., AL-ZAABI, Y., PICKUP, G., MACKAY, E., GOZALPOUR, F. & TODD, A. 2006. Simulation of CO2 storage in saline aquifers. *Chemical Engineering Research and Design,* 84, 764-775.

GREGORY, A. 1976. Fluid saturation effects on dynamic elastic properties of sedimentary rocks. *Geophysics,* 41, 895-921.

HAN, D.-H. & BATZLE, M. L. 2004. Gassmann's equation and fluid-saturation effects on seismic velocities. *Geophysics,* 69, 398-405.

HEINEMANN, N., WILKINSON, M., PICKUP, G. E., HASZELDINE, R. S. & CUTLER, N. A. 2012. CO2 storage in the offshore UK Bunter Sandstone Formation. *International Journal of Greenhouse Gas Control,* 6, 210-219.

HILL, R. 1963. Elastic properties of reinforced solids: Some theoretical principles. *Journal of the Mechanics and Physics of Solids,* 11, 357-372.

HOLLOWAY, S., VINCENT, C. J., BENTHAM, M. S. & KIRK, K. L. 2006. Top-down and bottom-up estimates of CO2 storage capacity in the United Kingdom sector of the southern North Sea basin. *Environmental Geosciences,* 13, 71-84.

IVANDIC, M., JUHLIN, C., LÜTH, S., BERGMANN, P., KASHUBIN, A., SOPHER, D., IVANOVA, A., BAUMANN, G. & HENNINGES, J. 2015. Geophysical monitoring at the Ketzin pilot site for CO2 storage: New insights into the plume evolution. *International Journal of Greenhouse Gas Control,* 32, 90-105.

IVANDIC, M., YANG, C., LÜTH, S., COSMA, C. & JUHLIN, C. 2012. Time-lapse analysis of sparse 3D seismic data from the CO2 storage pilot site at Ketzin, Germany. *Journal of Applied Geophysics,* 84, 14-28.

JOHNSON, D. L. 2001. Theory of frequency dependent acoustics in patchy-saturated porous media. *Journal of the Acoustical Society of America,* 110, 682-694.

KAZEMEINI, S. H., JUHLIN, C. & FOMEL, S. 2010. Monitoring CO2 response on surface seismic data; a rock physics and seismic modeling feasibility study at the CO2 sequestration site, Ketzin, Germany. *Journal of Applied Geophysics,* 71, 109-124.

KNIGHT, R., DVORKIN, J. & NUR, A. 1998. Acoustic signatures of partial saturation. *Geophysics,* 63, 132-138.

LEBEDEV, M., TOMS-STEWART, J., CLENNELL, B., PERVUKHINA, M., SHULAKOVA, V., PATERSON, L., MÜLLER, T. M., GUREVICH, B. & WENZLAU, F. 2009. Direct laboratory observation of patchy saturation and its effects on ultrasonic velocities. *The Leading Edge,* 28, 24-27.

LUMLEY, D. 2010. 4D seismic monitoring of CO2 sequestration. *The Leading Edge,* 29, 150-155.

MARGRAVE, G. F. 2003. Numerical Methods of Exploration Seismology with Algorithms in MATLAB.

MAVKO, G. & MUKERJI, T. 1998. Bounds on low-frequency seismic velocities in partially saturated rocks. *Geophysics,* 63**,** 918-924.

MAVKO, G., MUKERJI, T. & DVORKIN, J. 2009. *The rock physics handbook: Tools for seismic analysis of porous media*, Cambridge University Press.

NIVEN, R. K. 2006. Force stability of pore-scale fluid bridges and ganglia in axisymmetric and non-axisymmetric configurations. *Journal of Petroleum Science and Engineering,* 52**,** 1-18.

PEARCE, J. 2005. *Technology Status Review: Monitoring Technologies for the Geological Storage of CO2*, DTI.

PERMEDIA 2014. BOS, Version 5.1. *Halliburton, Ottawat, Ontario*.

REUSS, A. 1929. Berechnung der Fließgrenze von Mischkristallen auf Grund der Plastizitätsbedingung für Einkristalle. *ZAMM-Journal of Applied Mathematics and Mechanics/Zeitschrift für Angewandte Mathematik und Mechanik,* 9**,** 49-58.

SENGUPTA, M. & MAVKO, G. 2003. Impact of flow-simulation parameters on saturation scales and seismic velocity. *Geophysics,* 68**,** 1267-1280.

SINGH, V. P., CAVANAGH, A., HANSEN, H., NAZARIAN, B., IDING, M. & RINGROSE, P. S. 2010. Reservoir Modeling of CO2 Plume Behavior Calibrated Against Monitoring Data From Sleipner, Norway.

SMITH, T. M., SONDERGELD, C. H. & RAI, C. S. 2003. Gassmann fluid substitutions: A tutorial. *Geophysics,* 68**,** 430-440.

TAYLOR, C. & JULLIARD, F. 2013. An Introduction to Source Modelling and Wavelet Analysis Nucleus+.

TOMS, J., MÜLLER, T., CIZ, R. & GUREVICH, B. 2006. Comparative review of theoretical models for elastic wave attenuation and dispersion in partially saturated rocks. *Soil Dynamics and Earthquake Engineering,* 26**,** 548-565.

WHITE, J. 1975. Computed seismic speeds and attenuation in rocks with partial gas saturation. *Geophysics,* 40**,** 224-232.

WILLIAMS, J. D. O., JIN, M., BENTHAM, M., PICKUP, G. E., HANNIS, S. D. & MACKAY, E. J. 2013. Modelling carbon dioxide storage within closed structures in the UK Bunter Sandstone Formation. *International Journal of Greenhouse Gas Control,* 18**,** 38-50.

WILSON, M. & MONEA, M. 2004. IEA GHG Weyburn CO2 monitoring & storage project. Summary report 2000-2004.